Low-Speed Unsteady Aerodynamics of a Pitching Straked Wing at High Incidence—Part I: Test Program

R. G. den Boer*
National Aerospace Laboratory (NLR), Amsterdam, the Netherlands
and
A. M. Cunningham Jr.†
General Dynamics, Fort Worth, Texas

A low-speed wind-tunnel test on a straked delta wing, oscillating in pitch, was conducted in summer 1986 in a cooperative program between General Dynamics (Fort Worth) and the National Aerospace Laboratory of the Netherlands. This test was supported by the Flight Dynamics Laboratory of the Air Force Wright Aeronautical Laboratories. Measurements of unsteady overall airloads and pressure distributions were performed covering a wide range of incidences (−8–50 deg) and amplitudes (1–16 deg). Most test cases were carried out at a windspeed of 80 m/s. The zeroth and first harmonic of the pressures and overall loads were measured. Also, time recordings were made and stored for later study of higher harmonics, power spectra, and cross-correlation functions. At 30 m/s, visualization of the unsteady flow was performed using a smoke tube fixed to the model and a pulsating laser-light sheet. A limited number of runs with maneuverlike inputs were carried out. At these runs only time recordings of the balance signal were made. Part I presents the test setup and the procedures used in this test. In addition, some examples of the results are shown. Part II presents a first analysis of the data obtained during this experiment.

Nomenclature

b	= local wingspan, m
C_m	= wing pitching-moment coefficient, $= m/QSc_r$; reference axis at 73.27% of c_r (see Fig. 5)
C_N	= wing normal-force coefficient, N/QS
C_p	= pressure coefficient, $= (p-p_s)/Q$
$(C_p)_i$	= unsteady pressure coefficient, $= p_i/Q\Delta\alpha = \mathrm{Re}(C_p) + i\mathrm{Im}(C_p)$
$(C_p)_m$	= mean pressure coefficient
c	= local chord, m
c_r	= root chord, m
f, FREQ	= frequency, Hz
HARM	= harmonic component (HARM = 0: mean; = 1: first harmonic)
i	= SQRT(−1)
k	= see REDFR
l	= wing rolling moment, Nm (see Fig. 1)
MACH	= freestream Mach number
m	= wing pitching moment, Nm (see Fig. 1)
N	= wing normal force, Nm (see Fig. 1)
n	= wing yawing moment, Nm (see Fig. 1)
p	= pressure at model surfaces, Pa
p_s	= freestream static pressure
Q	= dynamic pressure, Pa
REDFR	= reduced frequency, $= \pi f c_r/V$
S	= wing area, m^2
T	= wing tangential force, N (see Fig. 1)
V	= freestream velocity, m/s
x	= chordwise coordinate, m (see Fig. 1)
Y	= wing force in y direction, N (see Fig. 1)
y	= spanwise coordinate, m (see Fig. 1)
z	= coordinate normal to x-y plane, m
α,ALPHA	= angle of attack, deg
$\Delta\alpha$, dα, DALPHA	= amplitude of pitching motion, deg
β	= angle of sideslip, deg
φ	= phase angle of pitching motion, deg

Subscripts

i	= unsteady
m	= mean

Received Jan. 13, 1988; revision received May 22, 1989.

*Research Engineer, Aeroelasticity Department.
†Senior Engineering Specialist, Computational Fluid Dynamics Group, Aerospace Technology, Fort Worth Division. Associate Fellow AIAA.

I. Introduction

A. Motive

TODAY straked wings are becoming common features of advanced fighter aircraft. The strakes are designed to generate vortices coming off from the highly swept leading edges that stabilize the flow and provide additional lift to high angles of attack. In this way, the strakes contribute much to high maneuverability.

The vortex lift capability of straked wings has been explored fairly well. Experimental data concerning aerodynamic loading are available for various planforms and Mach numbers. Advanced calculation methods to predict the vortex flow are maturing.

The knowledge of unsteady loading on straked wings is less developed, both in the cases where the loading is due to wing oscillations—as required for aircraft stability and flutter analysis—and in cases where fluctuations in the flow are induced by vortex burst (or vortex breakdown) as required for stall and buffet predictions. Taking the flutter analysis for example, common practice is that flutter clearance calculations for straked wing fighters are still based on attached flow without leading-edge vortices because of lack of adequate calculation methods for unsteady vortex flow being validated by experiment. The immediate question then arises if such a procedure

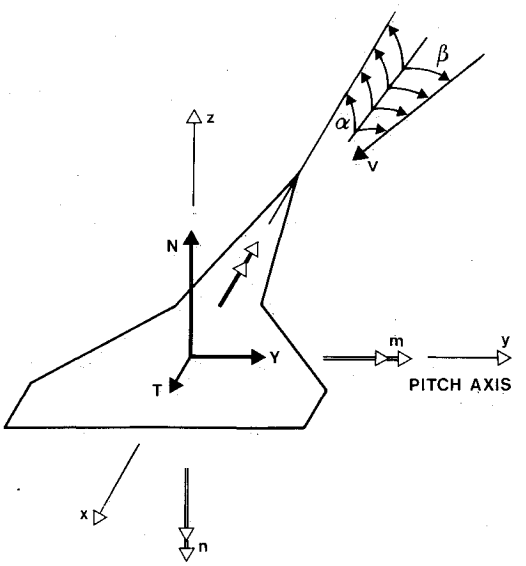

Fig. 1 Body-fixed axis system.

can guarantee sufficiently conservative predictions.

This situation has given rise to a cooperative project of General Dynamics and the National Aerospace Laboratory (NLR), with additional funding of the Air Force Wright Aeronautical Laboratories, concerning a wind-tunnel experiment with an oscillating straked wing. This experiment should extend the knowledge of unsteady vortex flow and provide a data base for the validation of computer codes for unsteady airloads. For a complete description of the test setup, procedures, and data base, the reader is referred to Ref. 1.

B. Some Physical Aspects

A brief description of some physical aspects of the unsteady vortex flow is given here. First, the main characteristics of the steady flow are considered. Figure 2 shows a straked wing under incidence. Vortices are coming off from the leading edges of the strake and the wing. The sharp strake leading edges generate vortex sheets at low incidence, which roll up spirally into the strake vortices and flow downstream over the wing. The vortices induce strong lateral velocities at the strake upper surface, giving rise to suction peaks at the position of the vortex cores (see upper-left inset). When the lateral velocities are large enough, secondary flow separations occur, leading to secondary vortices spiraling opposite to the primary vortices.

At moderate incidences, vortex sheets start to develop from the wing leading edges, starting at the kinks. As a result, the spanwise pressure distribution now shows two pressure peaks (see upper-right inset of Fig. 2).

At higher incidences, vortex burst or vortex breakdown occurs, starting with the wing vortices. An important consequence of vortex burst is that the corresponding suction peaks become weaker and the vortices lose their ability to produce additional lift. A normal behavior of vortex burst is that it will move upstream when the incidence increases. At still higher incidences, large-scale boundary-layer or stall separation occurs, starting often at the trailing edge.

The explanation of the preceding vortex flow becomes increasingly complicated in the case of interactions of strake and wing vortices, their influence on vortex burst and flow separation and, at high enough speeds, the presence of shock waves. The analysis of these phenomena is still the subject of many investigations.[2]

When the straked delta wing is oscillating, the strength and the position of the wing and strake vortex will also oscillate. As the vortices are being fed through the vortex sheets emanating from the leading edges, it is to be expected that the oscillations of the vortex strength and position will lag the wing oscillation. Phenomena such as vortex burst and stall separation have frequently shown hysteresis effects in steady measurements so that it might be conjectured that in the unsteady case these effects will cause an additional lagging.

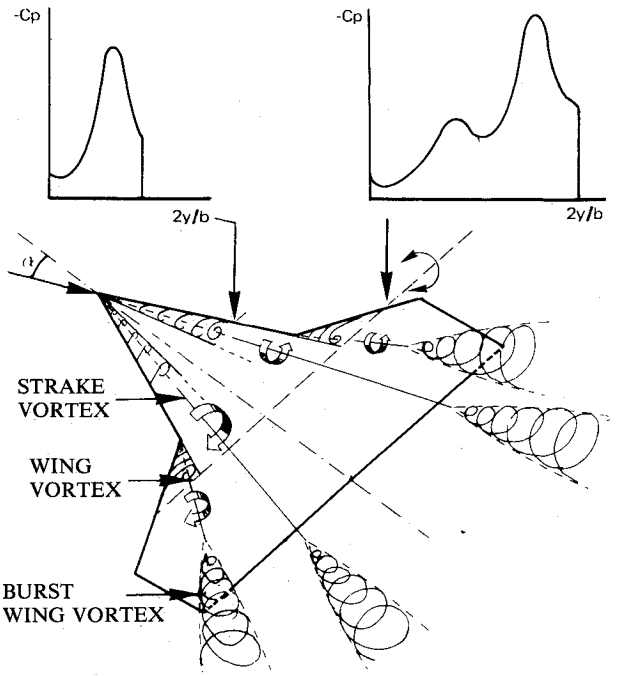

Fig. 2 Flow about a straked delta wing.

C. Objectives

The description of the problem area in Sec. I.A and of the various physical aspects in Sec. I.B leads to the following formulation of the objectives of the wind-tunnel experiment:

1) Obtain a physical insight of the vortex flow;

2) Set up a data base of unsteady aerodynamic data for computer code validation; and

3) Study the dynamic aspects of vortex bursts, up to high angles of attack at which vortex breakdown occurs close to the strake leading edge.

In achieving these objectives, some basic decisions were as follows:

1) The experiment was restricted to low speeds to keep the already complicated flow free from dominating compressibility effects. Continued experiments in the future might cover the higher speed range, especially the transonic range.

2) Preference was given to a balance to measure the overall aerodynamic loads, as it was expected that no practical grid of pressure pickups installed in the wind-tunnel model would be dense enough to provide accurate aerodynamic loads through integration because of the large pressure gradients. Measurements of pressure distributions would be applied only in a few strategically chosen sections.

3) The aerodynamic load and pressure measurements would be supplemented with information about the flow above the model upper side to study the position of the vortices, especially the vortex cores, development of vortex burst, etc. Application of a laser-light screen technique in a previous wind-tunnel test had already proven feasible[3] to study the position of the vortex cores (see Fig. 3). In addition, the means to apply a chopped laser-light screen were investigated.

II. Test Setup

A. Wind Tunnel

The tests were conducted in the NLR $3 \times 2.25\text{-m}^2$ low-speed wind tunnel situated in the Noordoostpolder.

The tunnel has a closed circuit and interchangeable test sections with a total length of 8.75 m. The test sections are pro-

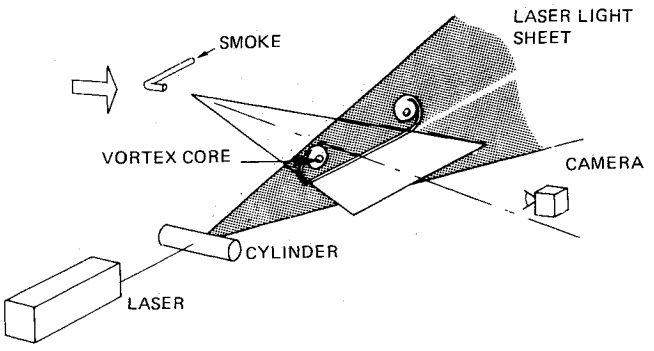

Fig. 3 Principle of laser-light sheet technique.

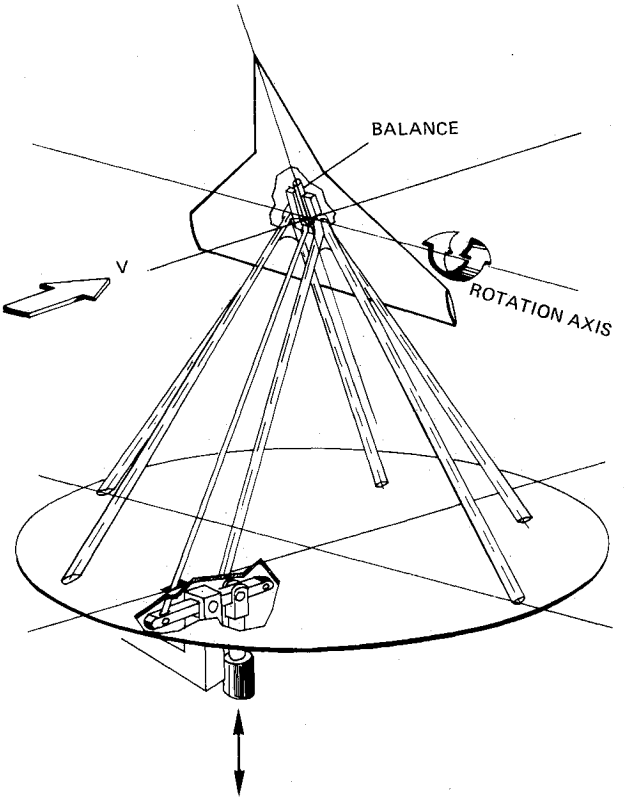

Fig. 4 Principle of test setup.

vided with turntables in the floor and ceiling. The tunnel has a maximum attainable windspeed of about 85 m/s.

B. Model and Model Support

An overall view of the test setup is shown in Fig. 4. The geometry of the model is indicated in Fig. 5. Because the model was not intended to represent a real aircraft, the parts that might complicate the aerodynamics, like fuselage and empennage, were left out. At the kink in the leading edge, where the strake passes into the wing, the thickness distribution was smoothed. The middle of the wing was thickened to accommodate the balance. The sides of this thicker region were rounded with a radius of 80 mm; the top of it was a flat surface. The model was designed and fabricated at NLR. It was made of a magnesium alloy to reduce inertia loads. The overall mass of the model, including its instrumentation, but without the balance, is 5.9 kg. The instrumentation is described in Sec. II.C. For the visualization tests, a smoke tube was attached to the lower side of the model, with its opening very close to the apex. The optimal position of the smoke tube was determined in a separate test, although during the final test the tube could be shifted in the x and z directions and its incidence could also be changed.

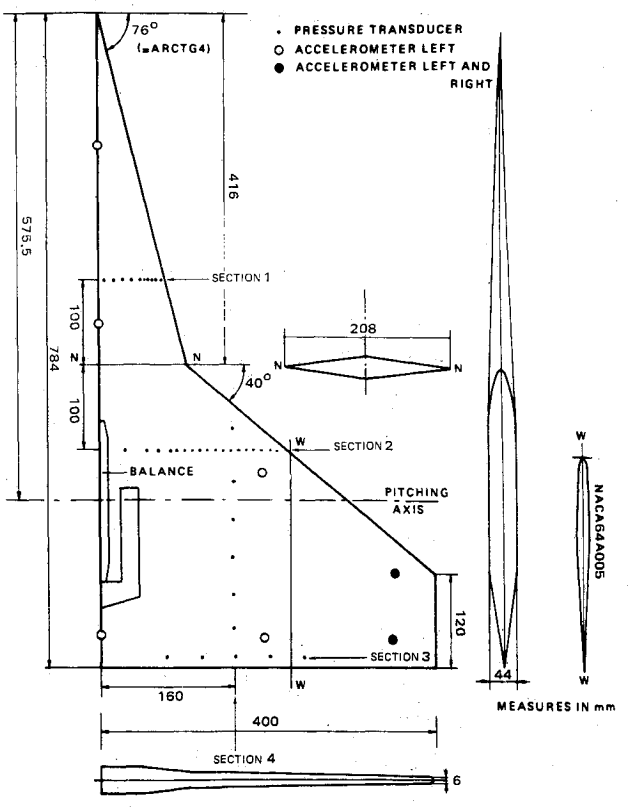

Fig. 5 Model instrumentation.

The support mechanism (see Fig. 4), also designed and built at NLR, was mounted on the turntable in the floor of the test section to enable model sideslip. By a system of struts, the model was supported such that it could perform a pitching motion about an axis at 73.3% root chord. The support elements were shaped aerodynamically. Two of them were used as a conductor for the instrumentation wiring.

C. Model Instrumentation

The instrumentation of the model consisted of a six-component balance, a displacement transducer, a temperature transducer, nine accelerometers, and 42 miniature pressure transducers. The location of the instrumentation in the model is indicated in Fig. 5.

For measuring the forces and moments, an existing six-component balance (NLR 635) was used. With this balance, forces and moments can be measured up to 450 N in tangential force, 1200 N in side force, 3000 N in normal force, 90 Nm in roll, 110 Nm in pitch, and 70 Nm in yaw.

With a linear variable differential transducer (LVDT) mounted between the model and the support, the oscillation amplitude and the mean steady wing incidence were measured. This provided the correct geometric incidence, which included the deformation of the balance.

The vibration modes were measured by nine accelerometers, located as indicated in Fig. 5.

The pressure transducers were mounted such that they were electrically isolated, free of local model deformation, and not influenced by the model accelerations. They were divided into four strategically chosen sections:

1) A spanwise section on the strake to collect data in the conical flow region (10 pressure transducers at $x/c_r = 0.4042$);

2) A spanwise section just behind the kink, showing the development of the leading-edge vortex starting from the kink (18 pressure transducers at $x/c_r = 0.6588$);

3) A spanwise section at the rear part of the main wing for measurement of buffet phenomena (eight pressure transducers at $x/c_r = 0.9682$); and

4) A chordwise section at the wing panel, showing the development of vortex burst as a function of incidence (eight pressure transducers at $2y/b = 0.4000$).

The sensitivity of the pressure transducers showed a small variation with temperature. By measuring the temperature of the model with a thermistor, the correct sensitivity of the pressure transducers could be applied.

D. Model Excitation

Excitation was provided by an electrohydraulic shaker system, which consisted of a hydraulic power supply, a combined linear actuator and servovalve, and a feedback control unit.[4] The hydraulic actuator could deliver a maximum static force of 13,000 N and a dynamic force of 8000 N at a total piston stroke of 35 mm at low frequencies to 16 mm at 16 Hz. The hydraulic actuator was suspended in a box and bolted rigidly to the turntable. The piston was connected to a crank, converting the linear motion to a rotational one. Using the excitation rod, this motion was transmitted to the yoke, which supported one side of the balance. On the other side of the balance, the model was clamped. During most runs, the model was forced into a sinusoidal motion. In a limited number of runs, a single pulse $(1-\cos)$ input was applied.

E. Equipment for Measurement of Overall Loads and Pressures

The wind-tunnel tests were performed using a computer-controlled multichannel transfer-function analyzer called PHAROS (Processor for Harmonic Analysis of the Response of Oscillating Surfaces). A description of this system is given in Ref. 5. The system is capable of analyzing incoming data from 48 channels simultaneously. Using a switch panel, this process was conducted twice, so that 96 different signals could be recorded.

Figure 6 shows a block diagram of the test setup, including the PHAROS system. The two-phase oscillator of PHAROS controlled a hydraulic actuator, which provided the model excitation. The response signals of the instrumentation were acquired by PHAROS for analysis. The electrical signals are fed through conditioners and transfer-function analyzers to obtain the zeroth-order component and the real and imaginary parts of the harmonic components. Next, these data were stored on a disk of the computer and a quick-look analysis was made. The analysis of each test run was performed in about 3 min, including plots and tables of all measured quantities. (See also Sec. IV.A.)

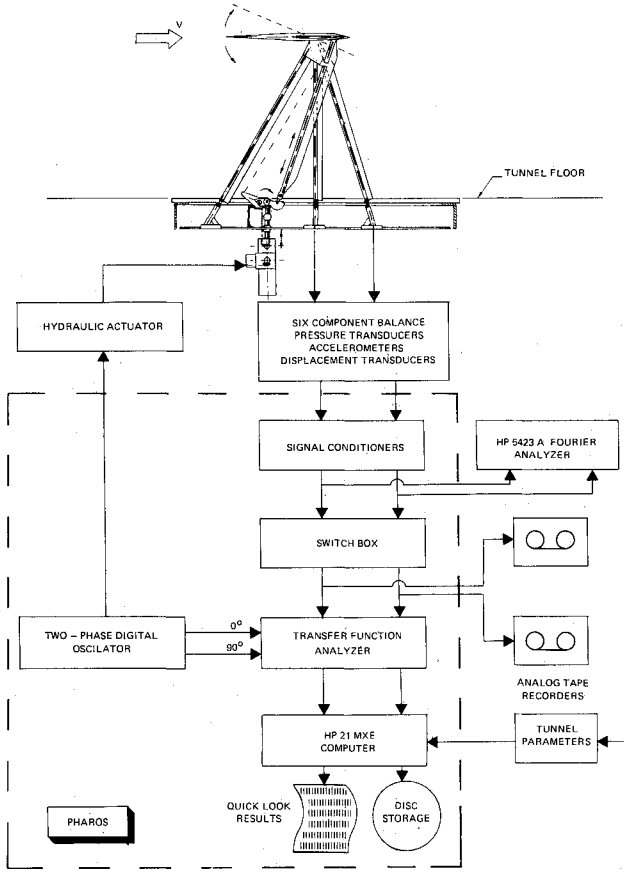

Fig. 6 Test setup for measurement of forces, moments, and pressures.

F. Equipment for Flow Visualization

Figure 7 shows a schematic overview of the visualization test setup. On the left-hand side, a top view is shown of the wind-tunnel test section with the wind-tunnel model in it and the flow-visualization equipment beside it. The smoke tube underneath the strake could inject smoke into the flow in the upstream direction. In this way, the smoke, mixed with air, was sucked into the vortices over the model. Using a 5-W argon-ion laser and a cylindrical lens, a light screen was formed that was perpendicular to the model when the model was at its mean incidence. The flow patterns were made visible by the light scattered by the smoke particles in the light screen, which is shown in the right side of Fig. 7.

To record the flow characteristics at fixed phase angles with respect to the model motion, a chopped laser-light screen was applied. Using an acousto-optic modulator, the laser-light screen was made intermittent. The modulator was controlled by a special device developed at NLR, which generated electronic pulses in pace with the same digital oscillator signal that controlled the model motion. The pulse signal was then converted to an amplitude-modulated high-frequency signal by a driver that excited the acousto-optic modulator. When no modulation was applied, the laser beam was interrupted by a mirror and reflected to a black absorber. In the case of 100% modulation, the modulator deflected the laser beam about 6 mrad. Next the beam passed the interrupt mirror and was led into the optical parts to produce the light screen using the cylindrical lens. The optical elements could be rotated about the optical axis to adjust the light screen perpendicular to the wing, when the model was at mean incidence.

At a distance of 2.50 m downstream of the rotation axis of the model, a photocamera was installed with its optical axis in the symmetry plane at the same level as the rotation axis of the model. The photographs were taken remotely controlled with a 250 filmback and a 100-mm lens. The photographs were taken mainly to determine the vortex core position at different phase angles of the model motion.

In addition, to enable the study of phenomena such as vortex burst, video recordings were made using a charge-coupled device (CCD) camera positioned beside the tunnel wall.

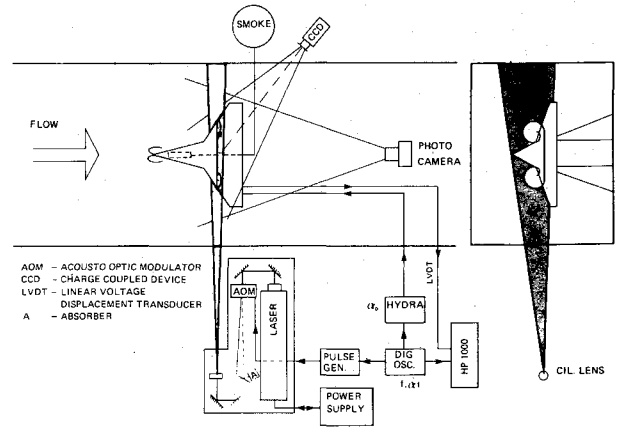

Fig. 7 Visualization test setup.

Table 1 Vibration modes with corresponding frequencies of the model (on the balance) and the support system

Mode no.	Frequency	Type
1	38.66	Roll
2	45.36	Roll + pitch
3	53.03	Pitch
4	111.87	Model bending
5	31.97	Yaw
6	80.03	Y displacement on support

III. Preparatory Tests

The model was supported by a structure consisting of several struts (see Fig. 4). To estimate the interference with the flow, steady measurements were performed in a separate preparatory test with the model suspended by wires to an overhead balance system.[6] Support interference corrections were derived, which were later applied in postprocessing the results of the main test.

In a separate test, the vibration modes of the model (on the balance) and the support system were measured. All resonance frequencies were far beyond the highest test frequency (see Table 1).

Another preparatory test was carried out to determine the optimal position of the smoke tube with respect to the model. Use was made of an oscillating dummy model with a smoke tube at varying positions. The test was performed in a small wind tunnel at the Delft University of Technology, Department of Aerospace Engineering, where a steady laser-light screen was applied. In this test, the optimal conditions for the smoke generation were also investigated.

The same dummy model was used in another wind-tunnel test in which the equipment and procedures for the unsteady flow visualization were tested.

IV. Procedures

A. Measurement of Overall Loads and Pressure Distributions

1. Transfer Functions

The main objective of these measurements was to establish the transfer function between the mechanical motion of the model as input and the pressures and overall loads as output. Using the PHAROS system (see Sec. II.E), the zeroth and first harmonics of the measured signals were determined.

These data were stored on the disks of the PHAROS computer. Next, the data of the balance were corrected for inertia effects and all quantities were normalized with the response of the displacement transducer at the model. Then a quick-look result of all measured quantities was produced on-line in tables and plots. The whole procedure of data acquisition and presentation took about 3 min for each test run. After the wind-tunnel test, the final data reduction of these harmonic data was made on the HP21/MXE computer of the PHAROS system. The following aerodynamic quantities were obtained.

1) One chordwise and three spanwise distributions of the mean steady pressure coefficients $(C_p)_m$;

2) One chordwise and three spanwise distributions of the unsteady pressure coefficients $\mathrm{Re}(C_p)$ and $\mathrm{Im}(C_p)$, normalized with the angular displacement of the wing derived from the output of the LVDT;

3) Zeroth and first harmonics of force and moment coefficients, measured with the NLR 635 balance, again normalized as mentioned earlier; and

4) Amplitudes and displacements, derived from accelerometer signals normalized with the displacement of the LVDT.

2. Time Recordings

In addition to the measurement of transfer functions, time recordings were made to enable the study of higher harmonics in case of strong nonlinearities, power spectra in case of vortex burst and strong stall effects, and cross-correlation functions in space and time in following the development of vortex burst and boundary-layer separation.

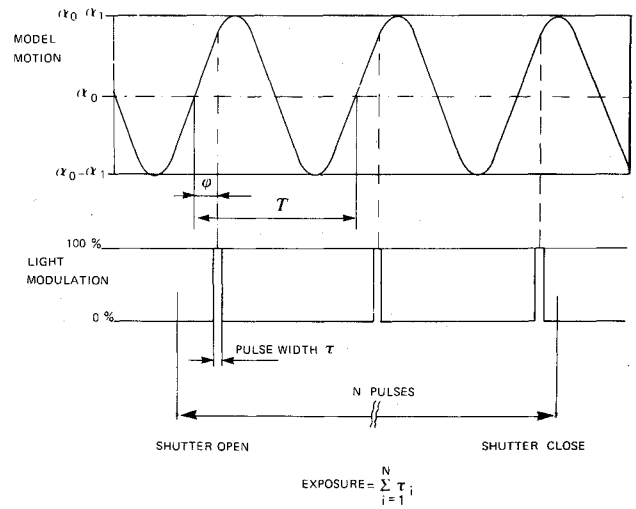

Fig. 8 Principle of visualization.

B. Incidence and Blockage

1. Incidence

The incidence measured by the LVDT was not influenced by the deformation of the balance. Therefore, the correct geometric incidence was obtained directly. However, as compared with free flight, the incidence was affected by the presence of the support system and the wind-tunnel walls. Therefore, a zero-lift correction was applied to correct for the influence of the support system and an upwash correction was applied to take the influence of the tunnel walls into account.

The zero-lift correction (-0.05 deg) is the difference in incidence at zero lift, between the steady tests in wires[6] and the steady tests on the strut support. In both tests, the wing model was equipped with wire suspension blocks.

The upwash correction according to the method of Refs. 7 and 8 was applied.

2. Blockage

As a result of the presence of the model in the test section, the effective dynamic pressure is increased by so-called "blockage" effects. The solid blockage can be neglected because of the small volume of the model. The wake blockage is caused primarily by the flow separation (bluff-body drag) and can be estimated from the lift-vs-drag curve according to the method of Refs. 7–9.

During the wind-tunnel test, the lift-vs-drag curve—determined previously for the model—suspended in wires,[6] was used to adjust the tunnel speed such that the dynamic pressure, corrected for blockage effects, was almost independent of the incidence.

C. Flow Visualization

The principle of the chopped laser light screen technique is shown in Fig. 8. The upper part of the figure shows the time history of the model motion, and the lower part shows the time history of the light pulses that generate the laser-light screen. The phase difference between model motion and the light pulses could be varied over the entire period of 360 deg.

Because the light screen was present only during a fraction of the cycle (2.2% maximum), several pulses were needed for one exposure. Consequently, the quality of the photographs taken was influenced by the total motion during the light pulses (depending on pitch rate and pulse width) and the time-averaging effect, i.e., the number of pulses needed for one exposure. This was not a serious drawback: in a preparatory test

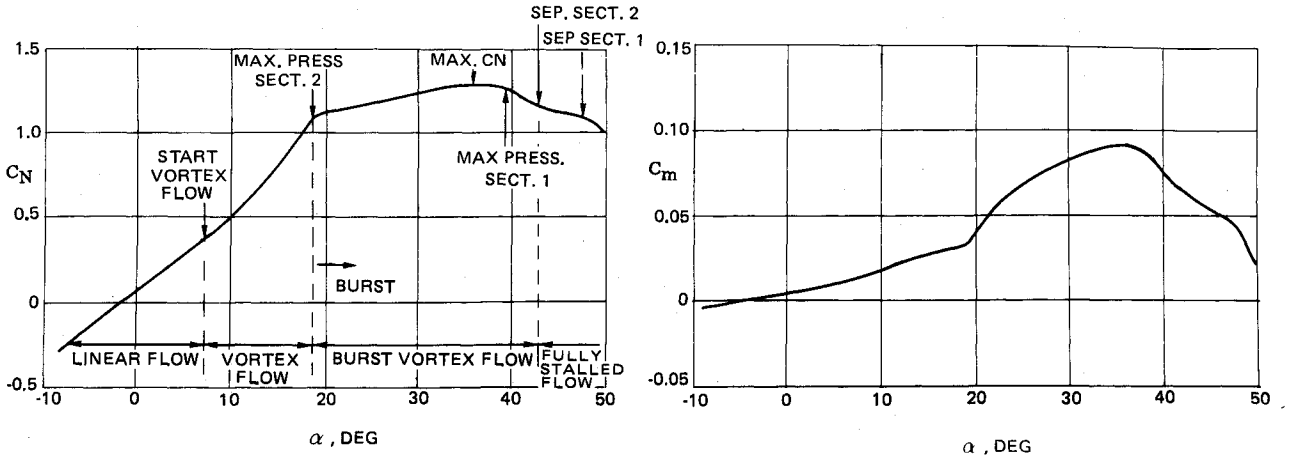

Fig. 9 Steady force data vs α.

(see Sec. III), the photographs taken were very suitable for determining vortex core positions at different phase angles of the model motion.

For qualitative information, the CCD video camera was used. This camera has a smaller resolution than the photocamera. However, because of the high sensitivity of the video camera, from each light pulse, a complete picture could be generated.

V. Test Program

A. Steady Tests

The steady tests, performed at zero sideslip and 80-m/s windspeed, covered an angle-of-attack range of −8–50 deg. To enable comparison with the steady test of the model suspended in wires,[6] the steady tests were performed with the model supported on the struts, with and without wire suspension blocks mounted in the wing. The influence of the wire suspension blocks had to be examined to determine their effect on the zero-lift correction (see Sec. IV.B.1).

B. Unsteady Tests

The unsteady tests covered a wide range of incidences (−8–50 deg), frequencies (1–16 Hz), and amplitudes (1–16 deg). Most of the pressure and load measurements were performed at 80-m/s windspeed with harmonic oscillation at reduced frequencies up to 0.5, based on root chord. At 80 m/s, runs with sideslip were also performed. In all of these runs with harmonic oscillation, the zeroth and first harmonics of the pressures and overall loads were measured, and time recordings were taped. In total, about 1000 runs with harmonic oscillation were performed.

In the results of the steady measurements (see Fig. 9), some characteristic incidence ranges can be distinguished: up to 8 deg-attached ("linear") flow; 8–19 deg—fully developed vortex flow; 19–38 deg—vortex burst extending from the trailing edge; and beyond 38 deg—vortex burst penetrating the strake, almost fully stalled flow.

Special emphasis was placed on incidences that marked transition of the flow characteristics or were typical for the flow characteristics in some incidence range. These incidences were 9, 19, 22, 36, and 42 deg. At these incidence values, a dense grid of amplitude and frequency was measured at 80 m/s. As an example, Table 2 shows the test matrix at 19-deg incidence. The influence of the windspeed was studied by repeating a number of runs at 55 and 30 m/s (same windspeed as in the visualization runs). The frequencies were adjusted at the same time to correspond with the reduced frequencies as applied in the 80-m/s runs. The visualization of the unsteady flow was performed at the five characteristic incidences, mentioned earlier.

During the visualization tests, the phase angle of the pulsation with respect to the model motion was varied over one complete cycle in 45-deg increments. At three chord positions, corresponding with the location of pressure transducers, at the five incidences mentioned earlier, and amplitudes and reduced frequencies that correspond with the 80-m/s runs, the smoke pattern in the light screen was registered on photographs and video. Over 1200 cases were completed.

In addition, some 80 runs with maneuverlike inputs were made. At these runs, only time records were made of the balance output.

Table 2 Test matrix at 19-deg incidence

	Δα						
f	2	4	6	8	10	12	14
2	X	X	X	X	X	X	X
3	X	X	X	X	X	X	X
4	X	X	X	X	X	X	X
5	X	X	X	X	X	X	X
8	X	X	X	X			
12	X						
16	X						

VI. Evaluation

For computer code evaluation, accurate overall loads are indispensable. A balance was used for this purpose, although it constituted a weak element in the support of the model. The balance signals were also affected by inertia loads. In this test, the resonance frequencies of the support system (including the balance) were far beyond the highest excitation frequency. Consequently, the influence of these vibration modes on the model motion was negligible. Because of the small inertia properties of the model and the low test frequencies, inertia loads were small. By measuring the model motion, correction for inertia loads could be made easily. In this way, overall loads were obtained that are expected to be more accurate

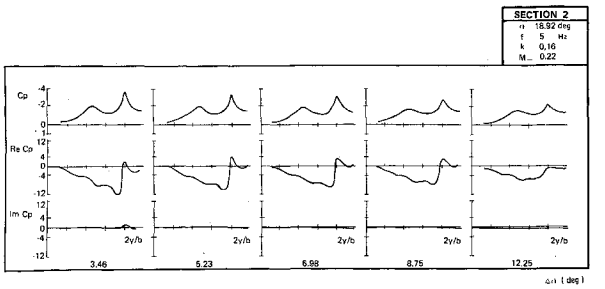

Fig. 10 Influence of amplitude on zeroth and first harmonic components of unsteady pressure distribution at section 2.

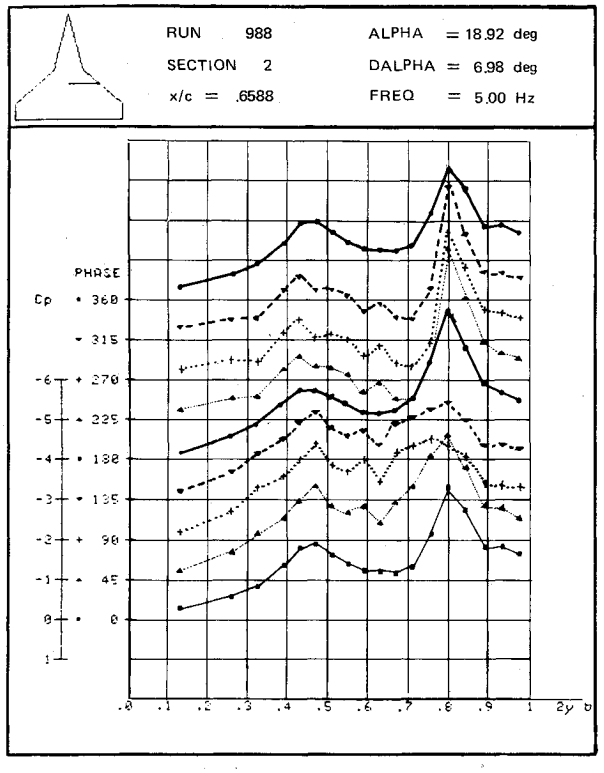

Fig. 11 Time history of pressure distribution at section 2.

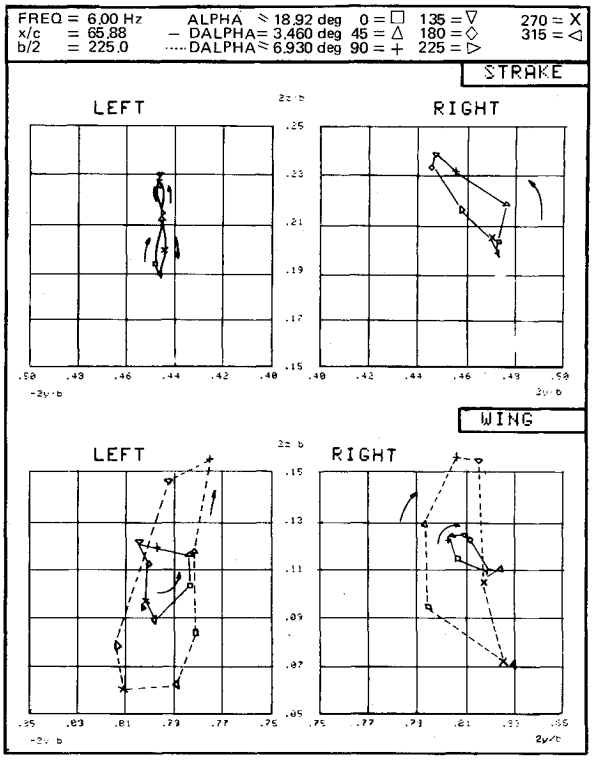

Fig. 13 Time history of vortex core position at section 2 (dashed lines correspond to photographs shown in Fig. 12).

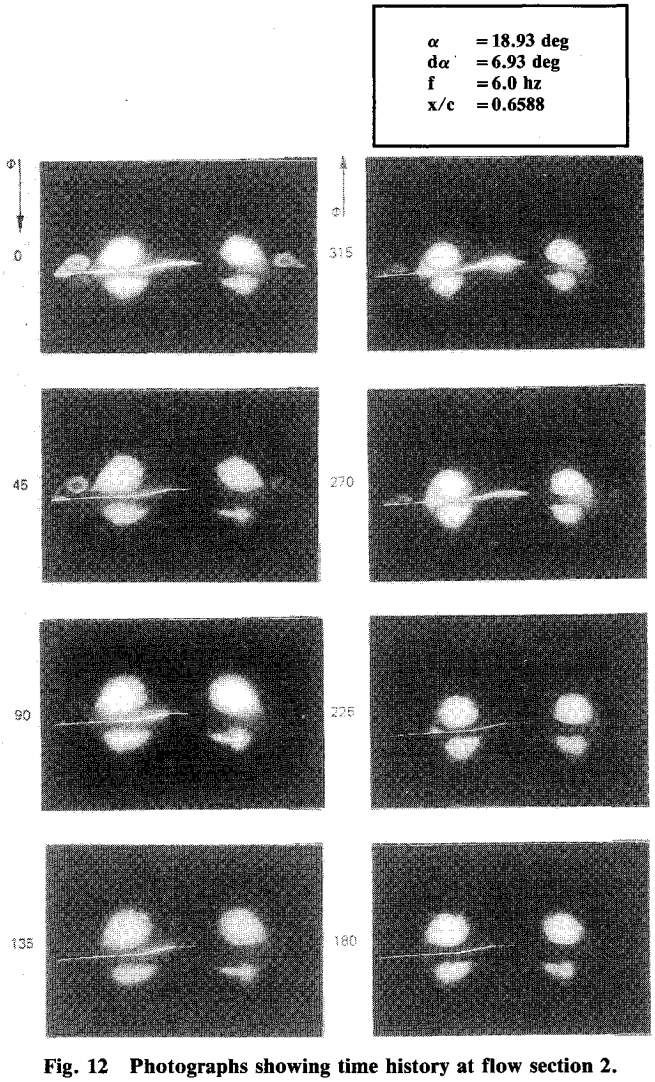

Fig. 12 Photographs showing time history at flow section 2.

than airloads obtained by integration of a large number of pressures measured at the model surface, especially in the presence of large pressure gradients.

The positioning of the pressure sections as indicated in Sec. II.C was a very appropriate one: information was obtained for many different types of flows. In the pressure section on the strake some pressure transducers were broken, probably as a consequence of the high acceleration level encountered in this section.

During the visualization at the three spanwise sections, a large number of photographs were taken with the aim of measuring the position of the vortex cores. This was not possible in all cases: especially in section 2 (just behind the kink), it was not always possible to inject the right quantity of smoke in both of the vortex systems—when much smoke was injected, the wing vortices could be photographed correctly but the strake vortices were overexposed; when less smoke was injected, the wing vortices could not be detected on the photographs. At the third section, the flow was burst in many of the tests and only qualitative information could be obtained from the photographs.

The video recordings provided much qualitative information on the flow, especially at vortex burst, because no time averaging over several light pulses was needed.

By using a step-by-step method in the test preparation, severe problems were avoided during the main test.

VII. Examples of Results

In Part II, an extensive analysis is presented of data obtained at the smaller amplitudes. Because a large number of runs are performed at higher amplitudes, in this part also some of the results of those runs are presented. Figure 10 shows an example of the influence of the amplitude on the pressure distribution at section 2. As one might expect, at the higher amplitudes the behavior of the flow is nonlinear. This is reflected in Fig. 11, which shows the history of the pressure distribution at section 2 at the same flow condition as Fig. 10. The pressure signal at the suction peak, which can be associated with the wing vortex (80% span), shows a nonlinear be-

havior, which is caused mainly by the presence of significant vortex and separated flows.

Figure 12 presents an example of the time history of the flow at section 2. The wing vortices are clearly visible, while the strake vortices are overexposed. Reflection of the light screen on the upper surface of the model gives an indication of the relative position of the vortex cores. In addition to qualitative information derived from the photographs, the position of the vortex cores is measured and presented in plots. Figure 13 shows an example that includes the values deduced from Fig. 12. As a reference, also the vortex core positions at half the amplitude are presented. At the smaller amplitude, the position of the strake vortices could also be determined. Note that the motion of the cores of the wing vortices varies nonlinearly with the amplitude of the model motion.

VIII. Concluding Remarks

The following goals, mentioned in Sec. I, have been achieved:

1) A large data base of both overall forces and moments as well as pressure distributions has been generated.

2) Quantitative information about the vortex core positions has been made available from photographs for study of the unsteady vortex flow.

3) Video and photograph documentation made during this experiment will contribute to enlarge the physical understanding of steady and unsteady vortex flows.

Acknowledgment

The test program discussed in this paper was funded partly under Contract F33615-85-C-3013 through the Flight Dynamics Laboratory of the Air Force Wright Aeronautical Laboratories. The monitor was Don W. Kinsey.

References

[1]Cunningham, A. M., Jr. and den Boer, R. G., "Unsteady Low Speed Windtunnel Test of a Straked Delta Wing, Oscillating in Pitch," AFWAL-TR-87-3098, Pts. I—VI, 1987.

[2]Boersen, S. J. and Elsenaar, A., "The International Vortex Flow Experiment, A Test Case for Compressible Euler Code Evaluation," National Aerospace Lab. Amsterdam, the Netherlands, NLR MP 86076 U, 1986.

[3]Kannemans, H., "Laser-Light Sheet Visualizations and In-Field Total Pressure Measurements in Steady Vortex Flow over Delta and Double Delta Wings," National Aerospace Lab., Amsterdam, the Netherlands, NLR TR 83057 L, 1983.

[4]Poestkoke, R., "Hydraulic Test Rig for Oscillating Wind Tunnel Models," National Aerospace Lab., Amsterdam, the Netherlands, NLR MP 76020 U, 1976.

[5]Fuykschot, P. H., "PHAROS, Processor for Harmonic Analysis of the Response of Oscillating Surfaces," National Aerospace Lab., Amsterdam, the Netherlands, NLR TR 77012 U, 1977.

[6]de Vries, O., "Force Measurements in a Low Speed Windtunnel on a Model of a Straked Wing, Suspended in Wires," National Aerospace Lab., Amsterdam, the Netherlands, NLR TR 86047 C, 1986.

[7]Maskell, E. C., "A Theory of Blockage Effects on Bluff Bodies and Stalled Wings in a Closed Windtunnel," Royal Aeronautical Establishment, England, UK, RAE Rept. Aero 2685, Nov. 1963.

[8]Garner, H. C., Rogers, E. W. E., Acum, W. E. A., and Maskell, E. C., "Subsonic Wind Tunnel Wall Correction," AGARDograph 109, 1966.

[9]Vayssaire, J. C., "Correction de blockage dans les essais en souffle effects des decollements," AGARD-CP-102.